

Applying Fisheye and Dual-Fisheye Camera in Rain Gauge Exposure Estimation

Peng, M.Y.^{1*} and Jaw, J.J.²

¹ Master Student, Department of Civil Engineering, National Taiwan University, Taiwan

² Associate Professor, Department of Civil Engineering, National Taiwan University, Taiwan

peng20000923@gmail.com

Abstract

A weather station should accurately represent the characteristics of its surrounding environment. To assess a weather station's suitability, it is essential to consider the spatial range that the meteorological instruments can cover, typically reflected by the exposure, which indicates the openness of the location. Before installing a rain gauge, it is necessary to assess the environmental exposure, as excessive obstruction can lead to inaccurate rainfall measurements. An omnidirectional camera is a camera with a 360-degree field of view in the horizontal plane, or with a visual field that covers a hemisphere or approximately the entire sphere. Using a camera with a wide-angle effect can quickly gather environmental information, making it an ideal tool for estimating the exposure of rain gauges. The image-based approach offers benefits such as low cost and simplified fieldwork as well. For estimating the exposure of rain gauges, this study employs a professional fisheye lens to provide rigorous and flexible methods and uses a dual fisheye camera to offer an adaptable method. The results demonstrate the suitability of these camera tools.

Keywords: Rain gauge exposure, Fisheye lens, Dual-fisheye camera, Image-based analysis

Introduction

The effect of the immediate environment upon the representativeness of the measurements obtained by meteorological instruments is considerable and is not always correctable. According to the “Guide to Meteorological Instruments and Observation Methods” issued by the World Meteorological Organization (2023), the instrument exposure of rain gauges is affected by factors such as the location, wind field, environmental shielding, and terrain, resulting in measurement deviations. Therefore, in order to ensure the reliability of the precipitation measurement results, it’s necessary to evaluate the openness of the rain gauge before installing it.

Figure 1 shows images taken with a camera positioned above a rain gauge, (a) to (d) showing the gradual reduction in sky openness, where surrounding structures increasingly obscure the sky. As shown in (d), when rain gauges are placed in such locations, insufficient exposure can seriously affect the accuracy of precipitation measurements. Lack of adequate exposure can lead to measurement errors and unreliable results because obstructions impede the gauge's ability to capture precipitation accurately.

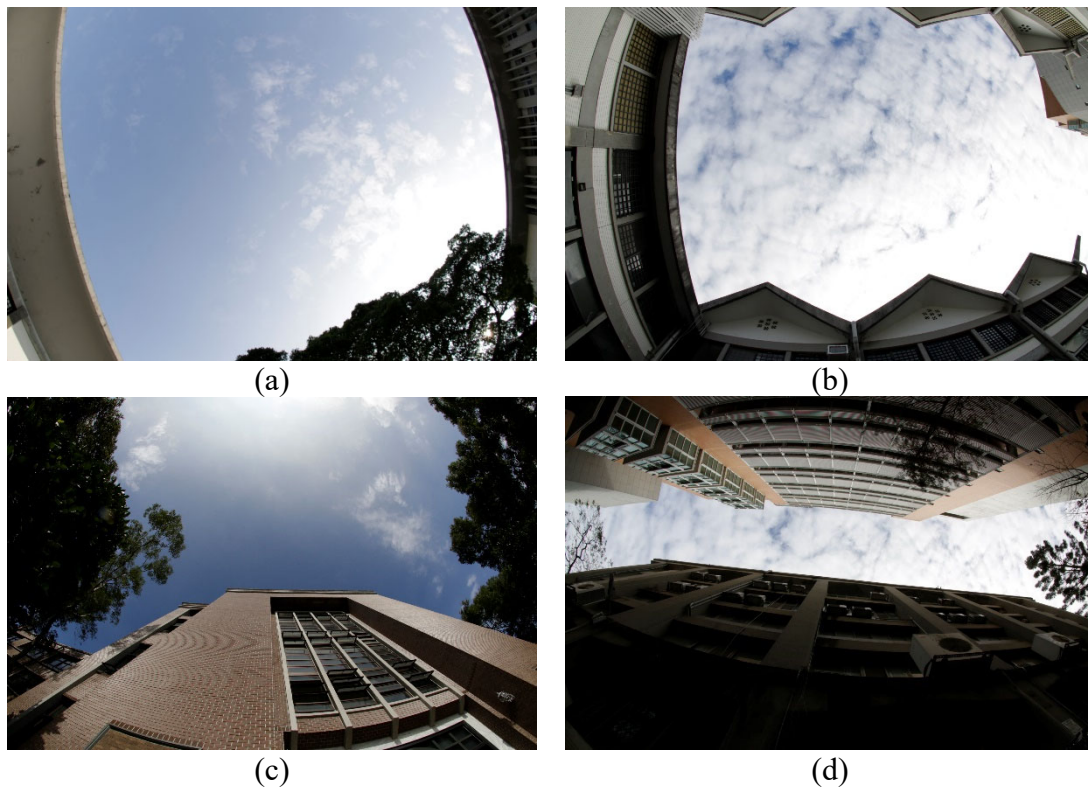


Figure 1: Sky openness

According to the "Guidelines for Meteorological Instruments and Methods of Observation" issued by the World Meteorological Organization, weather stations should be able to represent the characteristics of their surrounding environment. In order to evaluate the suitability of a weather station, it is necessary to consider the spatial range that the instrument can cover. The exposure of instruments such as meteorological observation platforms or rain gauges is usually used to reflect the openness of the field. Exposure is defined as the elevation angle from the center of the rain gauge to the upper edge of the surrounding shelter. It can be divided into four levels according to the level of openness, as recorded in Table 1. Based on the grading standards, the required angle precision for exposure measurement is approximately at the level of degree.

Table 1: Exposure Grading Standards (WMO, 2023)

Class	Angle	Description
Exposed site	0-5	Only a few small obstacles such as bushes, group of trees, a house
Mainly exposed site	6-12	Small groups of trees or bushes or one or two houses
Mainly protected site	13-19	Parkes, forest edges, village centres, farms, group of houses, yards
Protected site	20-26	Young forest, small forest clearing, park with big trees, city centres, closed deep valleys, strongly rugged terrain, leeward of big hills

This paper focuses on using fisheye images and panoramic images as the basis for exposure estimation. For the fisheye lens, both photogrammetry and computer vision methods are explored for camera calibration, offering rigorous and flexible approaches. For dual-fisheye cameras, the calibration procedure is omitted, rather establish a spherical coordinate system to calculate the exposure. The results from different algorithms and different camera types will be conducted for quality assessment and tool suitability analysis. The aim is to provide multiple application-level methods that reduce dependence on specific technical requirements and tool limitations.

Literature Review

A. Exposure Measurement

There are various methods for exposure measurement, including the hemispherical reflection projection method and the digital camera digitization method. As shown in Figure 2, the Kiff Mushroom Raingauge Exposure Meter is a polished hemisphere with a compass and concentric circles representing different exposure elevation angles. To estimate the environmental occlusion, the exposure meter is placed on the rain gauge, and a pen is used to trace the innermost edge of the surrounding environment's projection on the sphere. The exposure meter is a portable and flexible tool; however, the disadvantage is that it is difficult to digitize the exposure information and establish the database.



Source: Science Museum Group

Figure 2: Kiff Mushroom Rain gauge Exposure Meter

The more commonly used method is the digital camera digitization method. It only requires placing the camera on the rain gauge to take pictures of the sky and then applying suitable image processing to generate exposure information. As presented in Figure 3, the skyline of the image is set as the target object points to compute the exposure from the rain gauge center to surrounding obstacles.

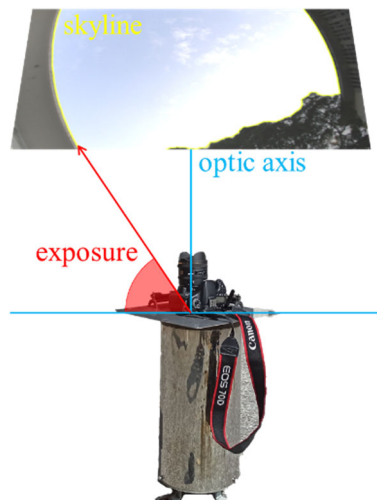


Figure 3: Digital camera digitization method

Servruk et al. (1994) have discussed the impact of wind fields and shading on rainfall capture in the Hellmann (Switzerland) area and proposed an annual rainfall correction plan. They have indicated that gauge site exposure (GSE) can fundamentally affect the magnitude of the wind-induced error and its correction. Lin et al. (2002) took an image of the sky above a rain gauge and used a total station to measure the elevation angles of several reference points. Utilizing the least-square method to obtain the conversion parameters between elevation angles and the distance on the image. Through direct conversion equation providing exposure information.

In addition, laser scanning is also a tool for exposure measurement. Pelc-Mieczkowska et al. (2015) used laser scanning to determine the shape and geometric relationships of obstacles within range. By measuring the distance, horizontal angles, and vertical angles between the instrument and the target, the three-dimensional coordinates of each measurement point are calculated based on these data to create the point cloud, to express the shielding conditions. The fisheye lens was also applied to model terrain obstacles at GNSS measurement points, compared with the result of laser scanning. The experimental results showed that the error of the fisheye image estimation method was two times higher than the laser scanning. However, Considering the cost of equipment and the time required for data acquisition and processing, using images as the basis for analysis still has its applicability.

B. Omnidirectional Camera

To evaluate instrument exposure, larger than or equal to 180-degree wide-angle cameras are needed. An omnidirectional camera is a camera with a 360-degree field of view in the horizontal plane, which may cover a hemisphere or approximately the entire sphere (Scaramuzza and Ikeuchi, 2014). See Figure 4, according to the camera's internal structure, it can be subdivided into three types. The first is a dioptric camera, which uses lenses with different multi-faceted structures to provide a field of view of approximately 180 degrees. The second type is the catadioptric camera, which combines a standard camera with a shaped mirror, such as a parabolic mirror, hyperbolic mirror, or elliptical mirror, to provide a 360-degree field of view in the horizontal plane and a field of view at an elevation angle of more than 100 degrees. The third type is a polydioptric camera, which achieves an approximately 360-degree field of view by combining multiple cameras with overlapping areas.

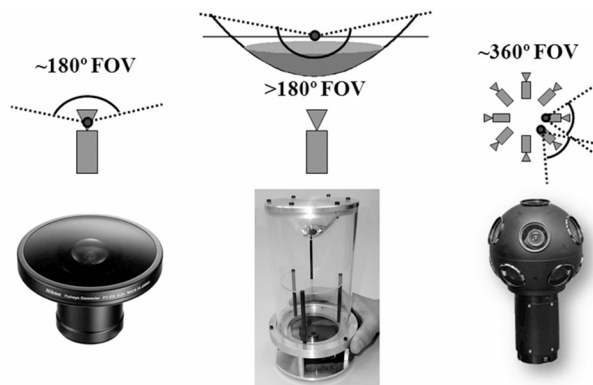


Figure 4: (a) dioptric camera (b) catadioptric camera (c) polydioptric camera

(Scaramuzza, 2021)

Among them, the catadioptric camera is difficult for the general public to obtain and use due to its complex imaging principles and high cost. Therefore, this type of camera is not suitable for exposure measurement.

C. Improvement Method

Exposure estimation can be conducted through multiple methods. However, considering equipment accessibility as well as labor and time costs, reducing fieldwork workload is also a key consideration. Using images as the basis for analysis presents a good choice. Images of the target area can be captured and then processed in the office to provide exposure information. Moreover, the image-based method does not require re-establishing the conversion mode due to site changes.

Methodology

A. Workflow

Figure 5 illustrates the workflow of this paper. The fisheye lens calibration includes both rigorous and flexible methods to determine the camera parameters, while a spherical coordinate system is established for the dual-fisheye to calculate the exposure. A quality assessment is conducted on all results, whether derived from different algorithms or tools. Finally, the suitability of these tools for exposure estimation is discussed.

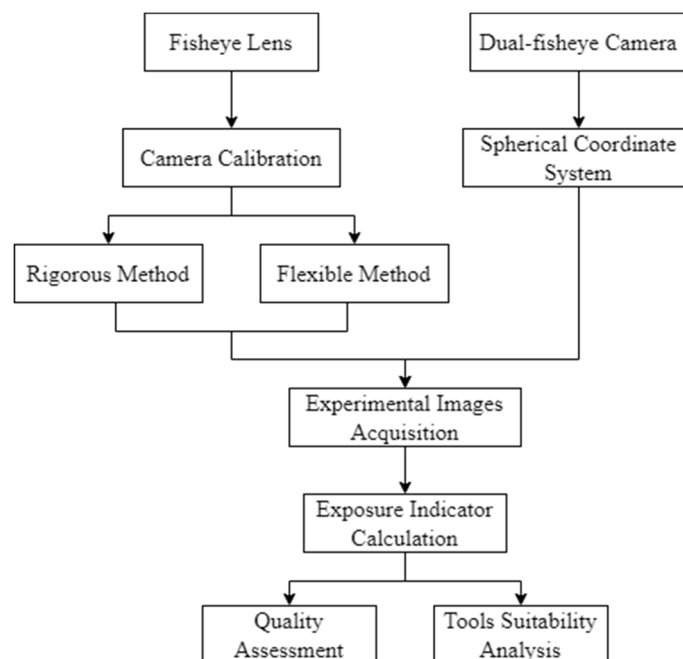


Figure 5: Workflow

B. Exposure Geometry

According to the World Meteorological Organization's definition of exposure indicator, the geometry and parameters are defined in Figure 6. The elevation angle θ , from the center of the rain gauge to the upper edge of the shelter, is defined as the exposure evaluation indicator. The calculation method of exposure is expressed as equation (1).

$$\theta = \tan^{-1} \left(\frac{fD + dr}{Dr} \right) \quad (1)$$

where:

- S camera perspective center
- O principal point
- P image point
- T rain gauge center
- r radial distance from image point to principal point
- f principal distance
- D horizontal distance
- d vertical distance from perspective center to camera placement plane

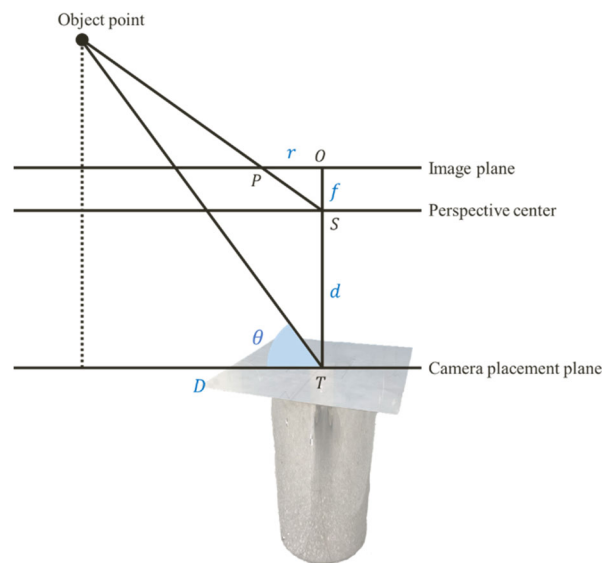


Figure 6: Exposure geometry

It should be noted that the geometry in Figure 6 is based on central perspective projection. However, this study employs a fisheye lens, which does not follow central perspective projection. As illustrated in Figure 7, the imaging point P_f is radially compressed inward compared to P , resulting in the corresponding elevation angle θ_f being smaller than the actual elevation angle θ . Additionally, lens distortion causes the actual image point to deviate from

the ideal one. Therefore, refinement of the image points and projection conversion are necessary to accurately determine the image point coordinates.

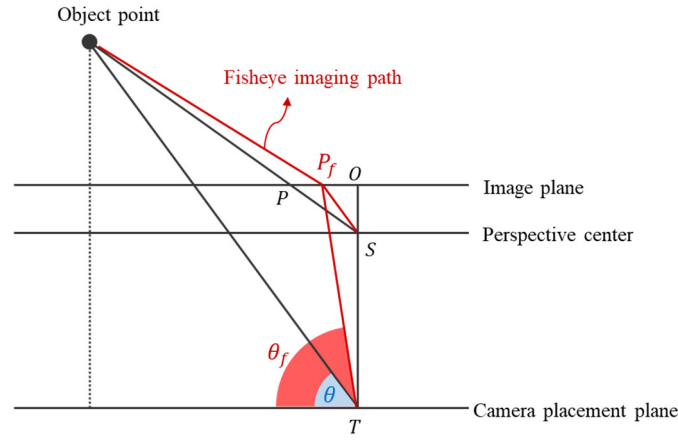


Figure 7: Projection conversion in exposure geometry

C. Fisheye calibration algorithm

The rigorous method uses the self-adaptive bundle adjustment with self-calibration method proposed by Yang (2019) as the fisheye calibration algorithm, utilizing the generalized least squares adjustment method to solve the unknowns. Referring to equation (2) taking equisolid-angle projection mode as an example, the object-image correspondence formula with additional parameters is set as the observation equation. Among them, the settings of the adjustment system are recorded in Table 2.

$$\begin{cases} x' = 2f \frac{\sin \left[0.5 \tan^{-1} \left(\frac{\sqrt{x^2 + y^2}}{z} \right) \right]}{\sqrt{\left(\frac{y}{x}\right)^2 + 1}} + x_h + \Delta x'_r + \Delta x'_d \\ y' = 2f \frac{\sin \left[0.5 \tan^{-1} \left(\frac{\sqrt{x^2 + y^2}}{z} \right) \right]}{\sqrt{\left(\frac{x}{y}\right)^2 + 1}} + y_h + \Delta y'_r + \Delta y'_d \end{cases} \quad (2)$$

where:

- x', y' image point under fisheye projection
- f principal distance
- x, y, z image point under central perspective projection
- x_h, y_h principal point coordinates
- $\Delta x'_r, \Delta y'_r$ radial lens distortion
- $\Delta x'_d, \Delta y'_d$ decentering lens distortion

As indicated from equation (3) to equation (6), the polynomial lens distortion model is used for image point refinement correction. (Brown, 1971; El-Hakim, 1986). r represents the radial lens distortion, K_1 to K_3 are the radial lens distortion parameters; d represents the decentering lens distortion, P_1 and P_2 are the decentering lens distortion parameters.

$$\Delta x'_r = x'(K_1 r'^2 + K_2 r'^4 + K_3 r'^6) \quad (3)$$

$$\Delta y'_r = y'(K_1 r'^2 + K_2 r'^4 + K_3 r'^6) \quad (4)$$

$$\Delta x'_d = P_1(r'^2 + 2x'^2) + 2P_2x'y' \quad (5)$$

$$\Delta y'_d = 2P_1x'y' + P_2(r'^2 + 2y'^2) \quad (6)$$

Table 2: Self-calibration adjustment system settings

	explanation	number
observations	coordinates of n points in m images	$2mn$
unknowns	exterior parameters object coordinates calibration parameters	$6m+3n+k$
redundancy		$2mn-6m-3n-k$

Additionally, the adjustment system introduces internal constraints to avoid the adverse effects of parameter solutions caused by the control point errors and coordinate system selection. Therefore, in addition to the original observation equations, seven datum equations were introduced.

$$\begin{cases} Be + A\xi = y, e \sim (0, \Sigma = \sigma_0^2 P^{-1}) \\ G^T \xi = 0 \end{cases} \quad (7)$$

where:

$$G^T = [G_{EOP}^T \quad G_{CT}^T]$$

$$G_{EOP}^T = \begin{bmatrix} 1 & 0 & 0 & 0 & 0 & 0 \\ 0 & 1 & 0 & 0 & 0 & 0 \\ 0 & 0 & 1 & 0 & 0 & 0 \\ 0 & -Z_L^i & Y_L^i & 1 & 0 & 0 \\ Z_L^i & 0 & -X_L^i & 0 & 1 & 0 \\ -Y_L^i & X_L^i & 0 & 0 & 0 & 1 \\ X_L^i & Y_L^i & Z_L^i & 0 & 0 & 0 \end{bmatrix} \quad G_{CT}^T = \begin{bmatrix} 1 & 0 & 0 \\ 0 & 1 & 0 \\ 0 & 0 & 1 \\ 0 & -Z_j & 0 \\ Z_j & 0 & Y_j \\ -Y_j & X_j & -X_j \\ X_j & Y_j & Z_j \end{bmatrix}$$

$$\forall i = 1, 2, \dots, m \quad \forall j = 1, 2, \dots, n$$

(Granshaw, 1980; Fraser, 1982)

Since the rigorous method requires a precise calibration field and operators with specialized knowledge, this paper proposes a more flexible method that may be better suited for practical applications. To explore alternatives to the calibration algorithm, both open-source and commercial software for fisheye lens calibration are examined.

OpenCV (Open Source Computer Vision Library) is an open-source software library designed for computer vision and machine learning. It was developed and released by Intel in 1999 to provide foundational tools and algorithms for computer vision applications. As indicated by equation (8), OpenCV adopts the Kannala-Brandt model (Kannala and Brandt, 2006) to describe fisheye distortion. This model focuses on a polynomial model of radial distortion, omitting the tangential distortion term. In the fisheye calibration module, multiple images of a checkerboard are required. The corner points are automatically detected, and their image coordinates, along with the corresponding object space coordinates, are used as input values. By establishing the conversion relationship between object space, image space, and camera coordinate system, the Levenberg-Marquardt algorithm is used to solve the camera parameters, which is refined by minimizing the projection error.

$$r(\theta) = \theta(1 + k_1\theta^2 + k_2\theta^4 + k_3\theta^6 + k_4\theta^8) \quad (8)$$

Agisoft Metashape software (Agisoft, 2024) employs the equidistant projection model for calibrating cameras and performing bundle adjustment using fisheye images. Equation (9) to equation (11) is the projection model of the fisheye calibration algorithm in Metashape.

$$x = \frac{X_C}{Z_C} \quad y = \frac{Y_C}{Z_C} \quad (9)$$

$$r = \sqrt{x^2 + y^2} \quad (10)$$

$$x_f = f \cdot x \cdot \frac{\tan^{-1}(r)}{r} \quad y_f = f \cdot y \cdot \frac{\tan^{-1}(r)}{r} \quad (11)$$

D. Projection mode conversion

Referring to Figure 7, the exposure geometry assumes that the imaging path follows central perspective projection, and the radial distance r is calculated from the image points of this system. Therefore, the image points of the fisheye system must be converted to the central perspective projection system. (x, y) represents the image points following central perspective

projection. r' describes the radial distance under fisheye projection. Equation (12) takes equisolid-angle projection mode as an example.

$$r = f \times \tan \left(2 \sin^{-1} \left(\frac{r'}{2f} \right) \right) \quad (12)$$

E. Exposure Estimation by Dual-Fisheye

The characteristic of the dual-fisheye camera is that it uses the front and back lenses to capture images and then outputs panoramic images; however, sometimes they can not provide the original image shot by a single lens. Since the panoramic image is the result of post-processing, most of the geometric information has been lost, making it difficult to calibrate the camera. Therefore, the camera calibration procedure is omitted, and the panoramic image is used as the analysis basis. By measuring the image point coordinates and converting them to spherical coordinates, the elevation angle with the perspective center as the origin can be calculated. Refer to Figure 6 to obtain the parameters D and d . The elevation angle can be calculated to take the center of the rain gauge as the origin, which is θ .

Following explain the calculation method and the formulas recoded in equation (13). Refer to Figure 8(a), the image coordinate system is based on pixels, and the origin is located in the upper left corner. Figure 8(b) is a spherical coordinate system with the unit of radians. (λ, φ) can be converted from the image point coordinates (x, y) and the image size (m, n) . Among them, φ can be regarded as the elevation angle from the perspective center as the origin to the scene point. If the horizontal distance D is known, it can be converted to the elevation angle θ from the rain gauge center as the origin to the scene point.

$$\begin{cases} \lambda = \left(x - \frac{n}{2} \right) \times \frac{2\pi}{n} \\ \varphi = \left(\frac{m}{2} - y \right) \times \frac{\pi}{m} \end{cases} \quad (13)$$

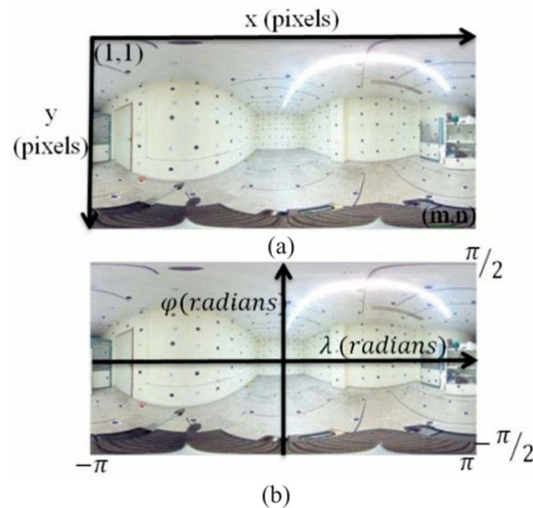




Figure 8: Coordinate systems, (a) image space coordinate system in pixel unit
(b) spherical coordinate system in radian unit (Aghayari *et al.*, 2017)

Results and Discussion

A. Camera Configurations

Table 3 documents the camera model and fisheye lens utilized in the experiment, along with the settings for the camera parameters.

Table 3: Fisheye camera specification

Category	Value	
Model	Canon EOS 70D	
Sensor Size	22.5×15 mm	
Resolution	1920×1280 pixels	
Pixel Size	0.0117 mm	
Lens	Sigma 10mm F2.8	
Principal Distance	10 mm	
Projection Mode	Equisolid-angle (Yang, 2019)	

For dual fisheye cameras, two types were used as exposure estimation tools in the experiment. The RICOH THETA SC system (Figure 9a) features a compact design, incorporating an internal reflecting prism that directs incoming light to the sensors (Figure 9b). This setup allows the lenses to be aligned with closely positioned entrance pupils, minimizing occlusion areas

due to the nearly coincident perspective centers. However, the use of optical reflective components may impact image quality (Castanheiro *et al.*, 2021).

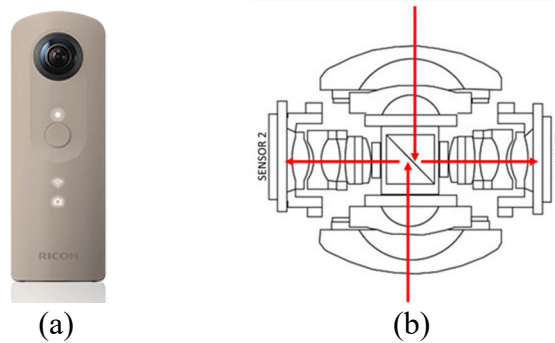


Figure 9: (a) RICOH THETA SC (Source: Ricoh360)

(b) set of lenses, internal cube, and both sensors (Campos *et al.*, 2018)

The GoPro MAX system (Figure 10) uses two separate lenses, however causing parallax for nearby objects and creating occluded areas, which leads to challenges in image stitching when generating panoramic images.



Source: GoPro

Figure 10: GoPro MAX (a) Side (b) Front (c) Back

Table 4 provides details on the dual-fisheye cameras used in the experiment, along with the camera parameter configurations.

Table 4: Dual-fisheye camera specification

Category	RICOH THETA SC	GoPro MAX
Sensor size	6.17×4.55 mm	6.17×4.55 mm
Sensor type	1/2.3" CMOS	1/2.3" CMOS
Principal distance	1.3 mm	3 mm
Resolution	5376×2688 (pixels)	4320×1440 (pixels)

The three cameras mentioned above were mounted on the rain gauge and took pictures of the surrounding scene. These images serve as the basis for exposure estimates.

B. Fisheye calibration results

a. Self-adaptive bundle adjustment with self-calibration method

The self-calibration method, which is defined as the rigorous method, requires precise control fields. All target codes arranged in the calibration site are measured at the total station, and 20 calibration codes and 25 check points are set. The distribution of calibration codes, check points, and perspective centers is plotted in Figure 11.

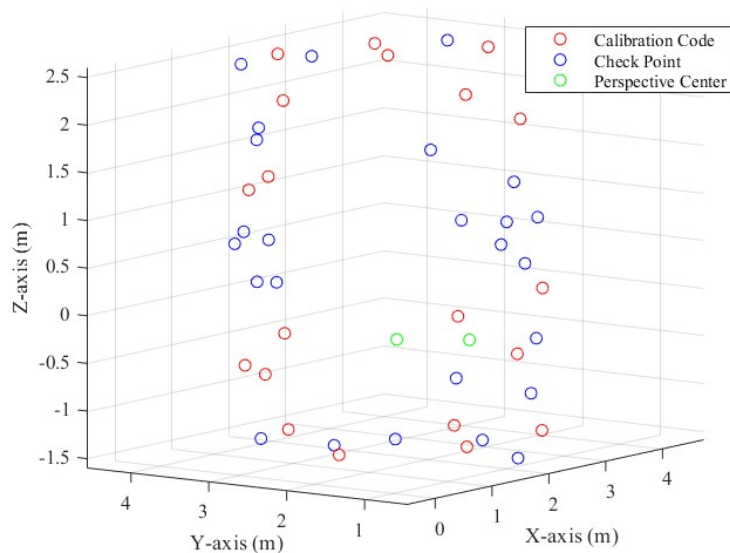


Figure 11: Three-dimensional point distribution

The calibration images are shown in Figure 12, and the points are marked on the images to illustrate the distribution. The method of obtaining the observations and setting the initial values of the unknown parameters is recorded in Table 5.

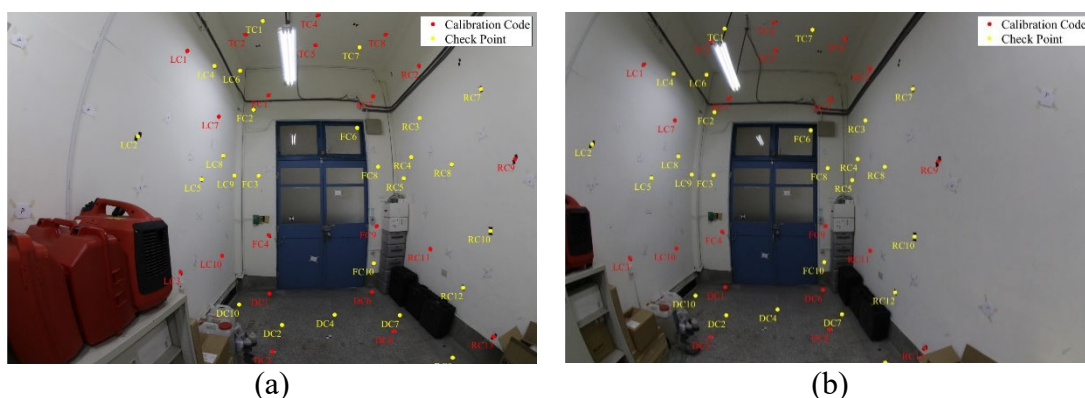


Figure 12: Calibration images (a) left Image (b) right Image

Table 5: Observations acquisition and unknowns initial values determination

Category	Parameters	Measure / Determinate
Observations	Image points coordinates	Measure manually
	Object points coordinates	Measure by total station
Unknowns	Exterior orientation parameters	Spatial resection
	Calibration parameters	$f = 10.3mm$, others set to zero

The results obtained from the self-calibration method are presented in Table 6. It is noted that the posterior unit weight standard deviation is 0.0050 mm, and the pixel size used for this calibration is 0.0117 mm. As a result, the calibration accuracy can be considered to have reached the sub-pixel level. Additionally, the radial and decentering lens distortion field is illustrated in Figure 13. The total lens distortion field overlay with calibration images is presented in Figure 14 as well.

Table 6: Calibration results and standard deviations

Parameters	Value	Standard deviation
$f(mm)$	10.3681	± 0.0098
$x_h(mm)$	-0.0066	± 0.0012
$y_h(mm)$	0.0079	± 0.0015
$K_1(1/mm^2)$	1.6489×10^{-5}	$\pm 5.1869 \times 10^{-5}$
$K_2(1/mm^4)$	-5.1806×10^{-7}	$\pm 8.5346 \times 10^{-7}$
$K_3(1/mm^6)$	7.5061×10^{-10}	$\pm 4.1317 \times 10^{-9}$
$P_1(1/mm)$	2.1769×10^{-5}	$\pm 1.1765 \times 10^{-5}$
$P_2(1/mm)$	-9.6316×10^{-5}	$\pm 1.4138 \times 10^{-5}$
$\hat{\sigma}_0(mm)$		0.0050

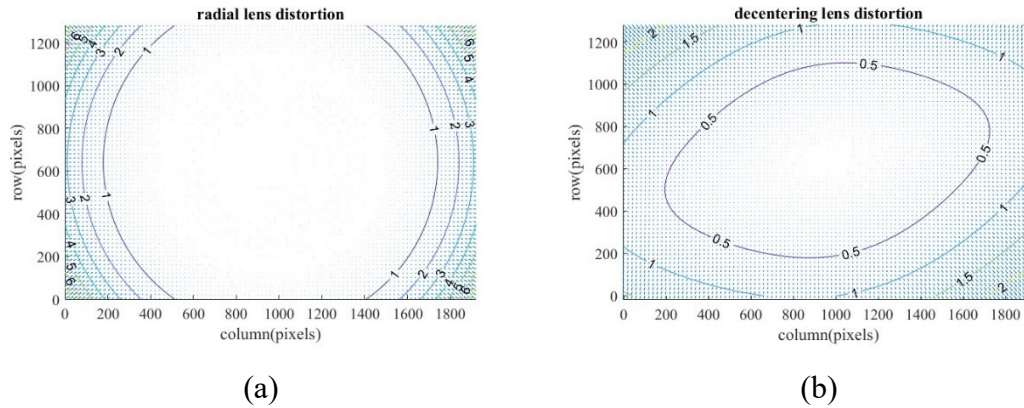


Figure 13: (a) radial lens distortion field (b)decentering lens distortion field

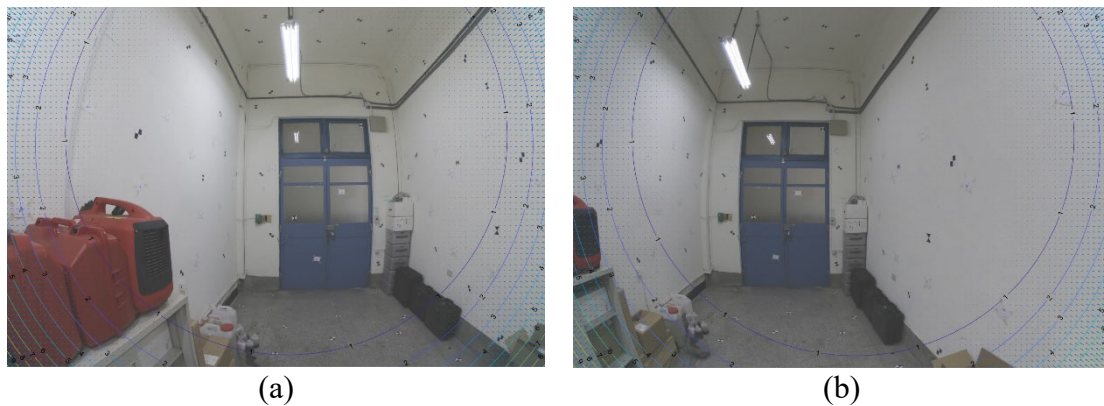


Figure 14: Total lens distortion field overlay with calibration images

(a) left image (b) right image

Moreover, through the object coordinates of the check points measured by the total station, the forward intersection can be performed after bundle adjustment, and the two can be compared to calculate the RMSE value. Referring to Table 7, the results explain that the solved interior orientation parameters can support millimeter-level positioning missions.

Table 7: Check points positioning accuracy

Check point $RMSE$	$RMSE_x$	$RMSE_y$	$RMSE_z$
Value(m)	0.0049	0.0084	0.0067

b. Metashape calibration result

Different from the rigorous method, Metashape does not require an accurate calibration field. Instead, it only requires capturing multiple images of the checkerboard from different angles. A set of 8 checkerboard images was acquired (see Figure 15) for the Metashape calibration process, it should be noted that the image must cover more than 10 squares on each side.

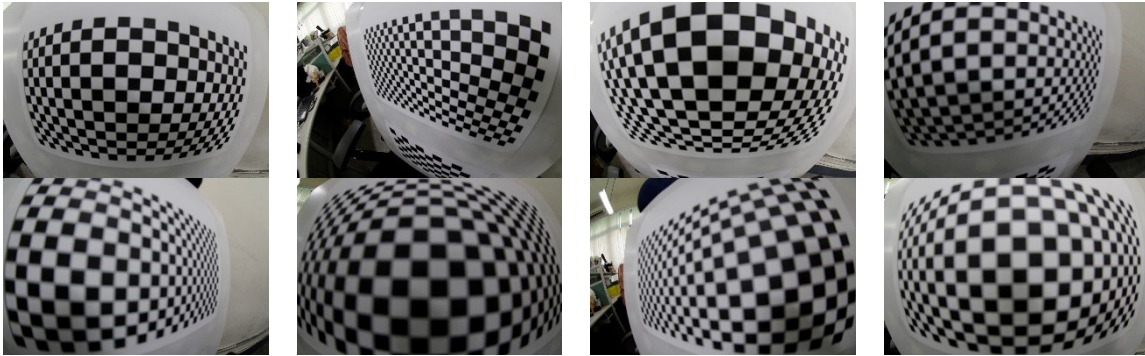


Figure 15: Calibration images for Metashape

The parameter values and errors of camera calibration using Metashape are recorded in Table 8, the original parameters are converted to millimeters using the method proposed by Hastedt et al (2016), making it easier to compare with the self-calibration result. The radial and decentering lens distortion fields are plotted in Figure 16. It can be observed that the radial lens distortion is greater compared to the rigorous method. This is because the Sigma 10 mm lens follows the equisolid-angle projection model, while Metashape's fisheye calibration algorithm uses the equidistant model. The difference in projection models is absorbed into the radial distortion, resulting in a larger magnitude of radial distortion in the Metashape calibration.

Table 8: Metashape calibration results and errors

Parameters	Original		Conversion	
	Value	Error	Value	Error
f	853.948	0.626	10.1532	0.0073
x_h	2.376	0.501	0.0283	0.0059
y_h	-2.108	0.353	0.0251	-0.0041
K_1	-1.85×10^{-2}	1.59×10^{-3}	-1.79×10^{-4}	1.53×10^{-5}
K_2	-2.12×10^{-3}	2.38×10^{-3}	-1.99×10^{-7}	2.21×10^{-7}
K_3	5.47×10^{-4}	1.10×10^{-3}	5.00×10^{-10}	9.87×10^{-10}
P_1	-6.04×10^{-4}	8.20×10^{-5}	5.95×10^{-5}	-8.05×10^{-6}
P_2	-5.65×10^{-4}	1.02×10^{-4}	-5.56×10^{-5}	1.00×10^{-5}

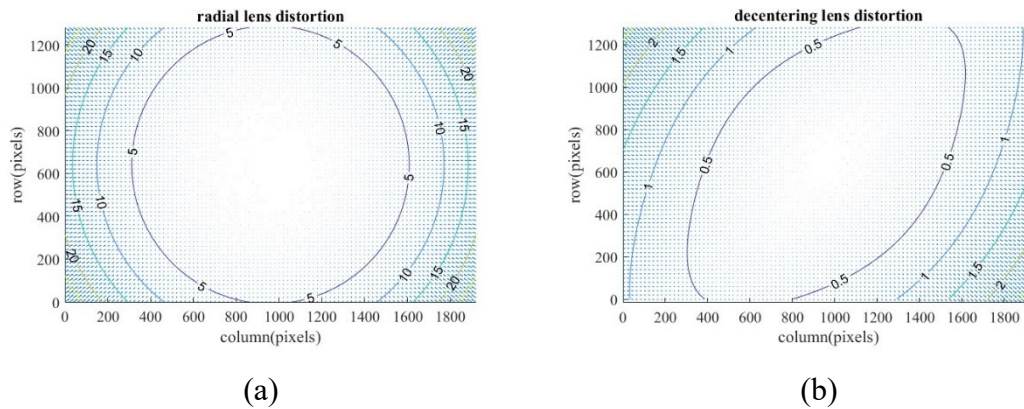


Figure 16: (a) radial lens distortion field (b) decentering lens distortion field

c. OpenCV calibration result

Similar to Metashape, an accurate calibration field is not needed, OpenCV also shoots the chessboard at different angles as calibration images. A set of 8 checkerboard images was acquired for the OpenCV calibration process, as presented in Figure 17. The intrinsic parameters and distortion coefficients are presented in Table 9.

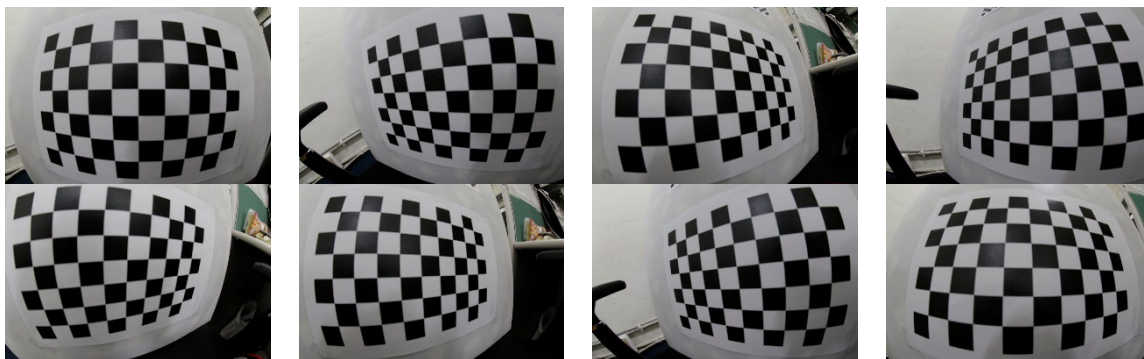


Figure 17: Calibration images for OpenCV

Table 9: OpenCV calibration results

Intrinsic parameters	Value (pixels)	Distortion coefficients	Value (dimensionless)
f_x	859.721	k_1	-0.019
f_y	858.707	k_2	-0.008
c_x	959.352	k_3	0.006
c_y	638.079	k_3	-0.001

As shown in Figure 18, the undistorted images are output by using OpenCV calibration results. The distortion of the images appears corrected when viewed with the naked eye. However, OpenCV does not provide quality indicators, accuracy of the calibration parameters cannot be assessed directly. Results can only be calculated and evaluated based on exposure later.

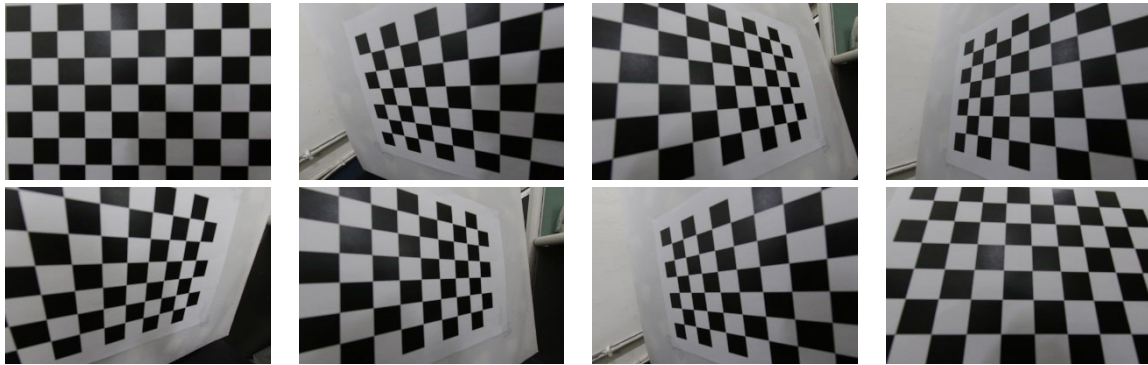


Figure 18: Undistorted images generated by OpenCV

C. Experimental images

There are two conditions set in this section. First, to ensure consistency in the starting point of exposure, all cameras were positioned above the rain gauge to capture images of the scene. Second, to eliminate uncertainties caused by weather conditions, control points were arranged in an indoor environment and used as targets for exposure calculation, the indoor experiment setting is displayed in Figure 19, which can be compared with Figure 3.

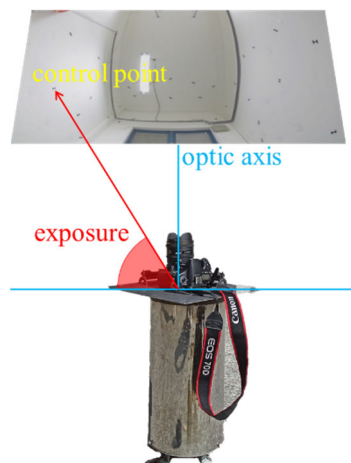


Figure 19: Indoor experiment setting

The camera placement as depicted in Figure 20, Sigma 10mm is placed flat above the rain gauge, and the optical axis is parallel to the zenith direction to capture the scene; RICOH THETA SC and GoPro MAX are placed upright above the rain gauge.

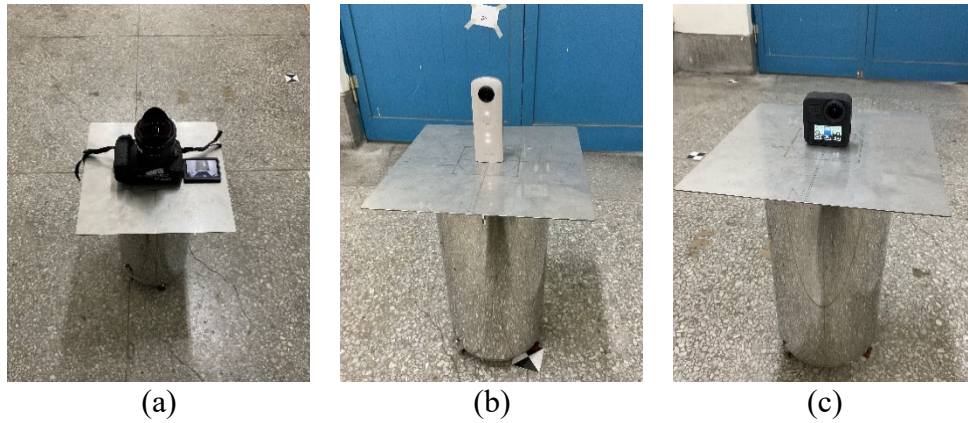


Figure 20: Camera placement (a) Sigma 10 mm (b) RICOH THETA SC (c) GoPro MAX

Figure 21(a) is the experimental image taken with Sigma 10 mm. It can be found that there are fewer control points in the image cover because the camera's optical axis is upward. Figure 21(b) presents the undistorted image the OpenCV fisheye module generated.



Figure 21: (a) original image (b) undistorted image

Figure 22 shows the panoramic image output by Ricoh Theta SC. It can be observed that the image covers a 360-degree field of view. However, in the zenith area, the area not directly facing the lens has greater deformation and lower definition.

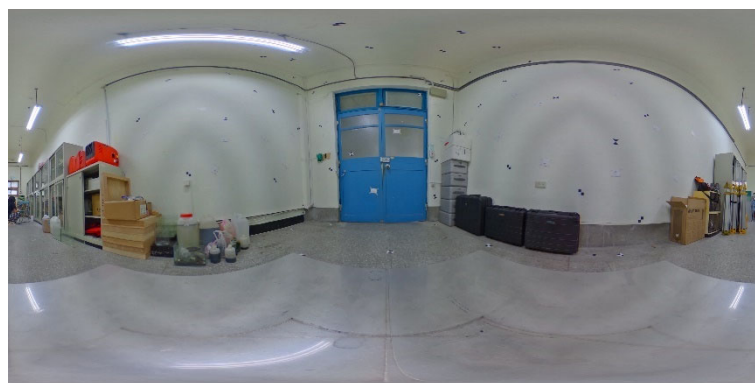


Figure 22: RICOH THETA SC experimental image

Figure 23 is a panoramic image output by GoPro MAX. It can be observed that the image does not cover the 360-degree field of view. Comparing the original image shot with a single lens (Figure 24), it can be found that the panoramic image is cropped before output, so it does not completely cover the zenith direction. Moreover, there are obvious traces of splicing on the panoramic image.



Figure 23: GoPro MAX experimental image



Figure 24: GoPro MAX original image shot by the single lens

D. Quality assessment

The scene includes 46 control points in total. Three cameras were used to capture images of the scene. The number of control points covered in the images is displayed in Table 10. The analysis of experimental results is divided into two parts. The first part involves capturing images with the Sigma 10 mm and applying camera parameters from different calibration algorithms to calculate exposure. The second part uses different cameras in the same scene to calculate exposure. Peng and Jaw (2024) demonstrated that the fisheye imaging described by rigorous object-image correspondence can provide below one-degree quality in exposure estimation. Therefore, the exposure values solved by the rigorous calibration method are set as the reference, and the other result would be compared with it.

Table 10: Number of control points image covered

	Sigma 10 mm	RICOH THETA SC	GoPro MAX
Number of control points	23	42	21
Intersection with Sigma 10 mm		27	9

First of all, the experimental image taken with the Sigma 10 mm lens (Figure 21a) was used to calculate the exposure angle using four different fisheye projection modes (see Figure 25). Among these, the equisolid-angle projection mode, which is the optimal mode for the Sigma 10 mm lens, was used as the reference value. Figure 26 shows the differences in exposure angle across the various modes. It can be observed that the results from the equidistant projection mode are the closest to the reference value, followed by the stereographic projection mode, with the orthographic mode showing the largest difference.

It is visible that the Sigma 10 mm fisheye lens is geometrically similar in both the equisolid-angle and equidistant projection modes, and the difference in the elevation angle calculations is within the allowable error range for exposure estimation. Therefore, for fisheye lenses with unknown projection modes, it is necessary to determine their optimal projection mode to meet the quality requirements for exposure estimation. This can be achieved either through calibration method 1 (rigorous method) or by mastering the imaging path via methods 2 or 3 (flexible methods).

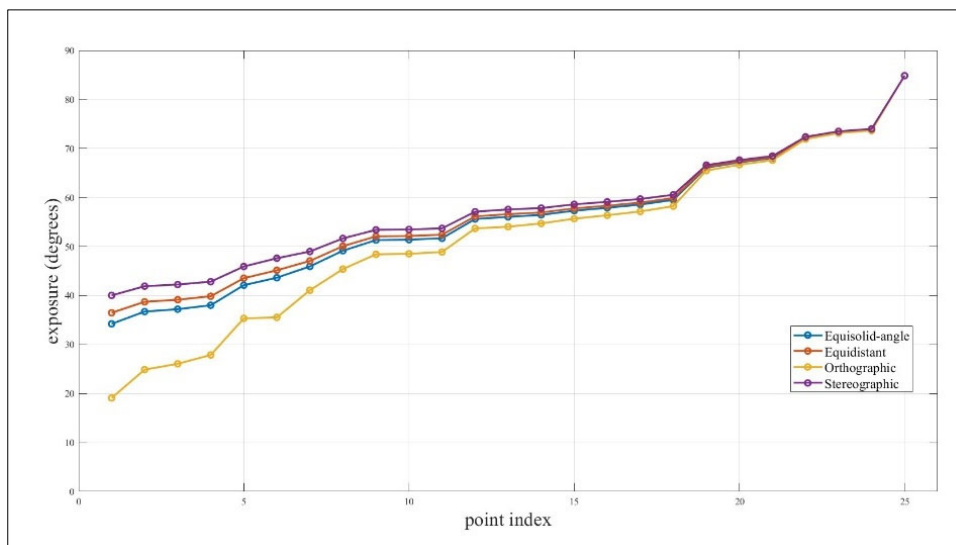


Figure 25: Compute exposure to different projection modes

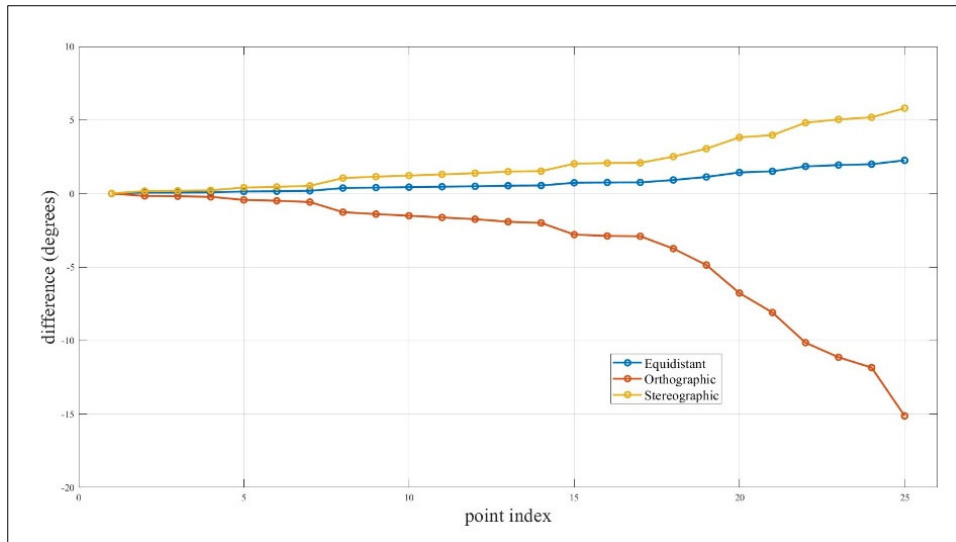


Figure 26: The difference between different projection modes and reference value

The exposure calculated using parameters solved by different calibration algorithms is plotted in Figure 27, "Reference" presents the results computed by the rigorous calibration method's camera parameters. The exposure values provided by the three algorithms are similar. Therefore, further displayed the differences between reference values and the other two values, as demonstrated in Figure 28. The statistical summary of exposure differences between different calibration algorithms is offered in Table 11 as well. It can be found that the results of OpenCV are relatively close to the reference values. While Metashape's results deviate more from the reference values, the difference remains under 0.7 degrees. This suggests that the flexible calibration method is also viable for exposure measurement.

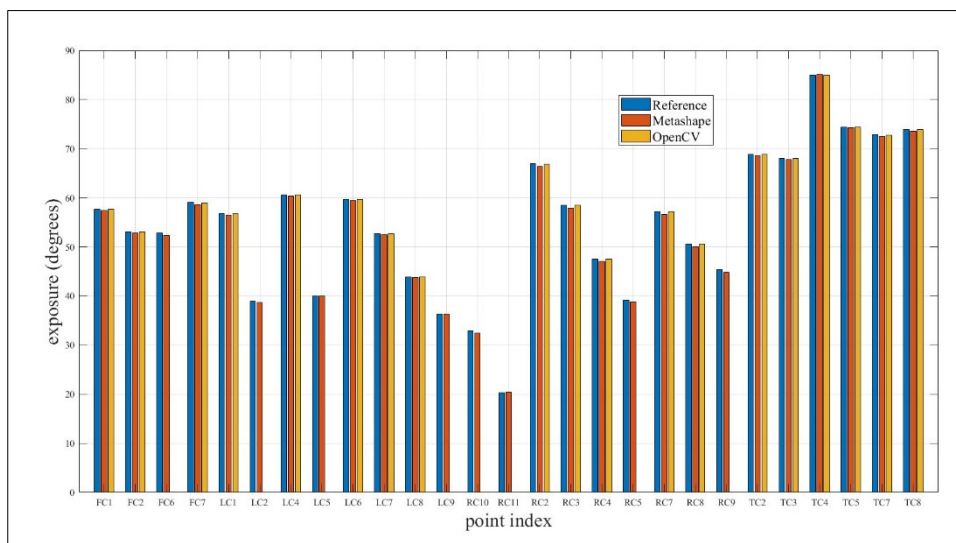


Figure 27: Exposure results of different calibration algorithms

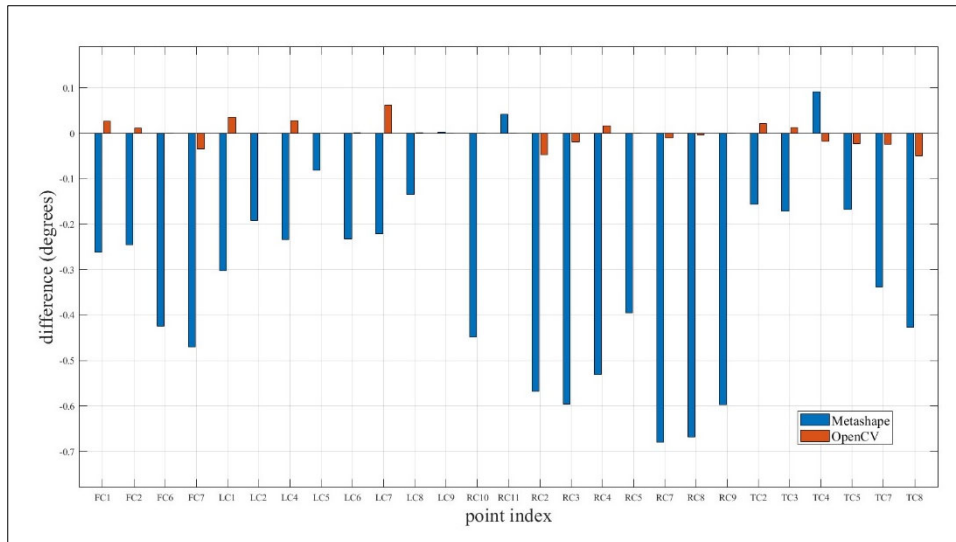


Figure 28: The difference from the reference value of different calibration algorithms

Table 11: Statistical summary of exposure differences between different calibration algorithms using Sigma 10 mm

	min	max	median	mean	RMSE
Metashape	-0.679	0.091	-0.262	-0.311	0.376
OpenCV	-0.049	0.063	0.002	0.000	0.029

(unit: degree)

Additionally, the results of assuming the fisheye lens operates only in the optimal projection mode without performing camera calibration have also been discussed. As displayed in Figure 29, "No calibration" indicates the exposure calculation result of only converting the fisheye projection to central perspective projection, in which the principal distance f is set to 10.3 millimeters. Figure 30 shows the difference between no calibration results and reference values, and the statistical results are recorded in Table 12 as well. It can be observed that the exposure estimation result without applying the calibration procedure can provide a quality of less than 0.6 degrees. The accuracy is better than applying the non-optimal projection mode (Metashape).

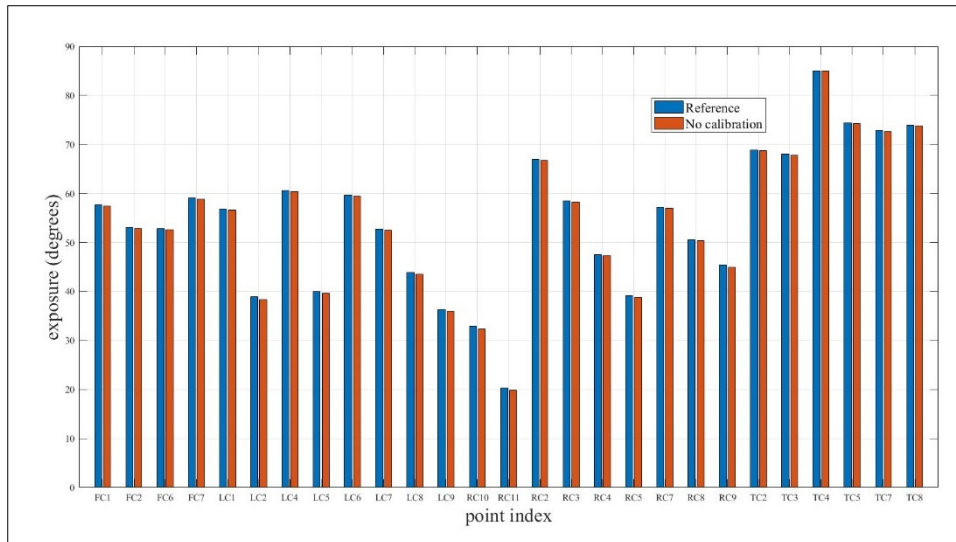


Figure 29: Exposure results of lens distortion correction

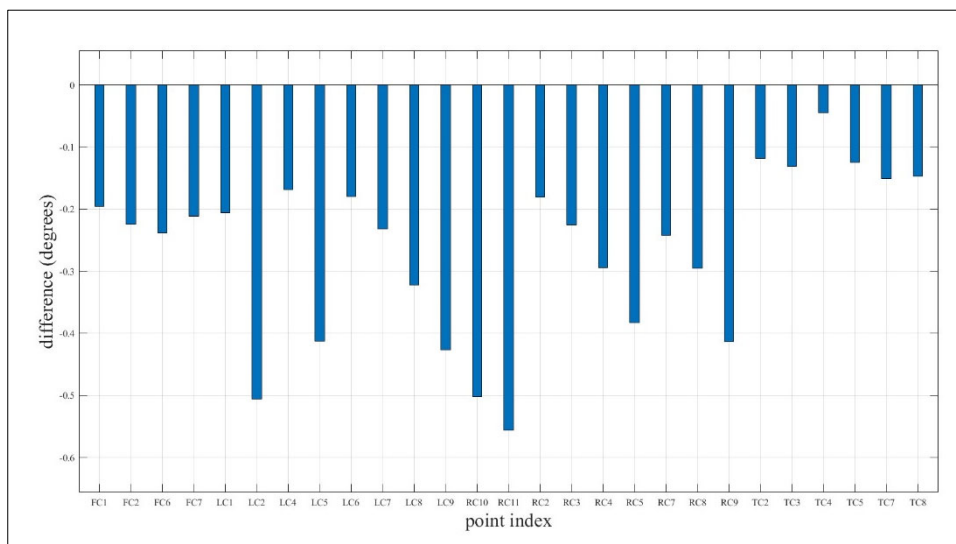


Figure 30: The difference between no calibration result and reference value

Table 12: Statistical summary of exposure differences of no calibration result

min	max	median	mean	RMSE
-2.840	-0.022	-1.771	-1.664	1.838
(unit: degree)				

Figure 31 shows the exposure calculation results of the three cameras. The horizontal axis is the point index and the vertical axis is the exposure with the unit of degrees. It can be found that the values of Sigma 10 mm and RICOH THETA SC are similar, while the results of GoPro MAX are far different. It is speculated that the camera structure and imaging principle are not

suitable for establishing a spherical coordinate system. Therefore, GoPro MAX cannot use the same method to calculate exposure as the RICOH system. The quality of the Ricoh Theta SC results, which are relatively close in value, will be further discussed.

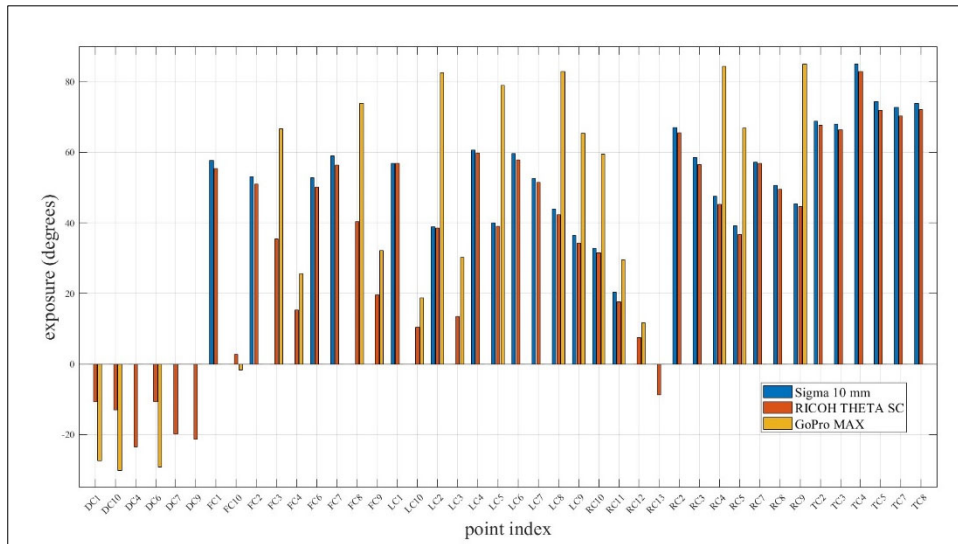


Figure 31: Exposure calculation of different cameras

The difference between RICOH THETA SC and the reference value is indicated in Figure 32, and the statistical results are recorded in Table 13. The maximum difference between the results of the RICOH THETA SC and the reference values is approximately 2.8 degrees, with a minimum difference of 0.2 degrees and an average of 1.6 degrees.

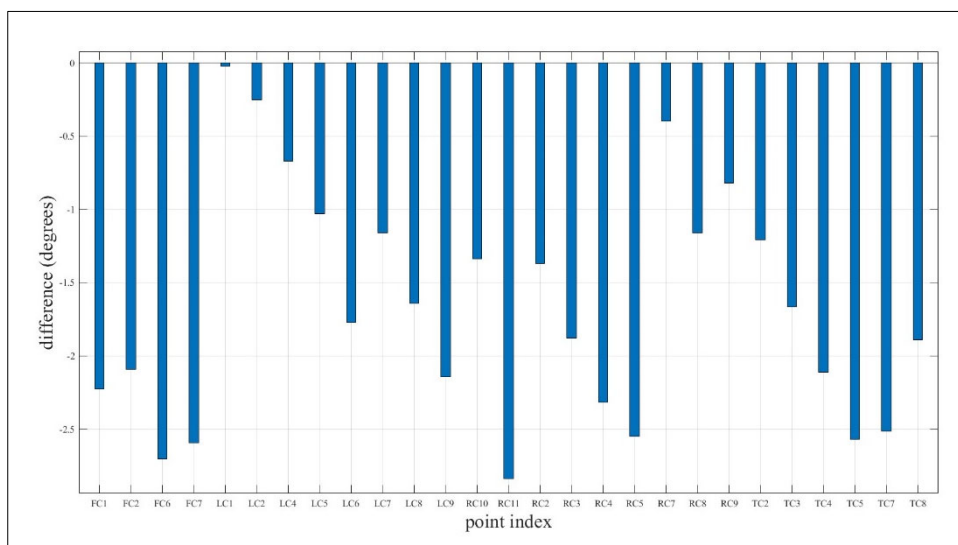


Figure 32: The difference between RICOH THETA SC and the reference value

Table 13: Statistical summary of exposure differences by RICOH THETA SC

min	max	median	mean	RMSE
-2.840	-0.022	-1.771	-1.664	1.838
(unit: degree)				

Figure 33 marks the exposure differences of each control point on the panoramic image generated by RICOH THETA SC. It can be found that there is a large amount of difference in the center area of the image, which is the area facing the front lens. This is likely due to the camera's structure, where light is redirected through reflectors. The reflective cube inside the dual fisheye camera may impact image quality by altering the light path and potentially increasing optical errors between the lens and sensor, resulting in a greater amount of distortion in the central area.



Figure 33: Deviation from reference values marked on RICOH image

By using dual fisheye cameras to estimate exposure in the same scene, two summaries can be drawn. First, the panoramic images produced by GoPro MAX are spliced and cropped, which results in the loss of some geometric information. Additionally, due to its imaging principle, converting the spherical coordinate system cannot be applied for exposure measurement. A separate method should be developed for GoPro MAX. Second, although the performance of the RICOH dual-fisheye camera in estimating exposure is not as accurate as that of professional fisheye lenses, as well as the angle precision does not reach the one-degree level, the dual-fisheye camera remains a viable tool for providing an adaptive method. This is largely due to its lower technical requirements and the fact that it does not require camera calibration.

Conclusion and Recommendation

The main purpose of this paper was to evaluate the substitutability of the fisheye calibration algorithm and try to estimate the rain gauge exposure by using different types of cameras. Since this application does not require high-precision positioning quality, the experiment used open-source and commercial software as the fisheye calibration algorithm. The results show that the flexible calibration method is suitable for exposure measurement. In addition, Metashape uses the equidistant model to calibrate the fisheye lens, while the fisheye lens used in this paper is the equisolid-angle projection. The exposure value calculated using Metashape calibration parameters differs from the reference value by less than 0.7 degrees, confirming the applicability of the projection mode of this application. Moreover, applying the optimal projection mode without lens distortion correction can provide a quality of less than 0.6 degrees, which is better than the Metashape result that is calibrated but uses a non-optimal projection mode.

Additionally, this paper explores the use of dual-fisheye cameras for estimating exposure. Although the accuracy is lower compared to professional fisheye lenses, dual-fisheye cameras remain viable tools for exposure measurement, as they eliminate the need for calibration procedures and have lower technical complexity. However, it is important to consider the type of dual-fisheye camera being used. The results indicate that the RICOH system can establish a spherical coordinate system for exposure calculation, while the GoPro system does not support this capability.

In future work, exploring other tools such as a fisheye attachment for smartphones is recommended. Due to its accessibility and portability, it has the potential to become a competitive option. Furthermore, since neither the rain gauge nor the camera has leveling and centering equipment, the eccentricity and tilt caused by the camera placement should be regarded as errors and corrected. The corresponding correction method still needs to be formulated.

References

Aghayari, S., Saadatseresht, M., Omidalizarandi, M., & Neumann, I. (2017). Geometric calibration of full spherical panoramic Ricoh-Theta camera. *ISPRS Annals of the Photogrammetry, Remote Sensing and Spatial Information Sciences; IV-1/W1*, 4, 237-245.

Agisoft. (2024). Agisoft Metashape User Manual - Professional Edition, Version 2.1.

Campos, M. B., Tommaselli, A. M. G., Marcato Junior, J., & Honkavaara, E. (2018). Geometric model and assessment of a dual-fisheye imaging system. *The Photogrammetric Record*, 33(162), 243-263.

Castanheiro, L. F., Tommaselli, A. M. G., Campos, M. B., & Berveglieri, A. (2021). Adaptive weighting of image observations for self-calibration with fisheye images. *ISPRS Annals of the Photogrammetry, Remote Sensing and Spatial Information Sciences*, 1, 81-87.

Fraser, C. S. (1982). Optimization of precision in close-range photogrammetry. *Photogrammetric Engineering and Remote Sensing*, 48(4): 561-570.

GoPro. (n.d.). *GoPro MAX*. <https://gopro.com/en/us/shop/cameras/max/CHDHZ-202-master.html>

Granshaw, S. I. (1980). Bundle adjustment methods in engineering photogrammetry. *The Photogrammetric Record*, 10(56): 181-207.

Hastedt, H., Ekkel, T., & Luhmann, T. (2016). Evaluation of the quality of action cameras with wide-angle lenses in UAV photogrammetry. *The International Archives of the Photogrammetry, Remote Sensing and Spatial Information Sciences*, 41, 851-859.

Lin, P. H., Hsu, C. I., & Juang, J. H. (2002). Case study on the deviation of surface precipitation measurement caused by wind deformation. *Atmospheric Sciences*, 30(3), 241-257. (in Chinese)

Pelc-Mieczkowska, R., Janicka, J., Bednarczyk, M., & Tomaszewski, D. (2015). Comparison of selected data acquisition methods for GNSS terrain obstacles modeling. *Acta Geodynamica et Geomaterialia*, 12(3), 307-315.

Peng, M.Y., & Jaw, J.J. (2024). Estimating sky openness for rain gauge based on fisheye lens. 2024 International Symposium on Remote Sensing, Taichung, Taiwan.

Ricoh360. (n.d.). *RICOH THETA SC*. <https://theta360.com/cn/about/theta/sc.html>

Scaramuzza, D. (2021). Omnidirectional camera. In *Computer vision: A reference guide* (pp. 900-909). Cham: Springer International Publishing.

Science Museum Group. (n.d.). *Kiff mushroom raingauge exposure meter* (Object No. 2005-63). Science Museum Group Collection Online. Retrieved September 9, 2024, from <https://collection.sciencemuseumgroup.org.uk/objects/co8061605/kiff-mushroom-raingauge-exposure-meter>

Sevruk, B. & Zahlavova, L. (1994). Classification system of precipitation gauge site exposure: evaluation and application. *International journal of climatology*, 14(6), 681-689.

Yang, H., 2019. Strategy formulation of fisheye lens calibration using the object-image correspondence based on geometric projection models. Master Thesis, National Taiwan University, Taiwan, ROC. (in Chinese)

World Meteorological Organization, 2023. Guide to Instruments and Methods of Observation. 2023 edition, WMO-No. 8, Geneva.